Crystal Structure of Wild-Type Tryptophan Synthase Complexed with the Natural Substrate Indole-3-glycerol Phosphate†

Michael Weyand and Ilme Schlichting*

Max-Planck-Institute for Molecular Physiology, Department of Physical Biochemistry, Otto-Hahn-Strasse 11, D-44227 Dortmund, Germany

Received September 1, 1999; Revised Manuscript Received October 4, 1999

ABSTRACT: We used freeze trapping to stabilize the Michaelis complex of wild-type tryptophan synthase and the α-subunit substrate indole-3-glycerol phosphate (IGP) and determined its structure to 1.8 Å resolution. In addition, we determined the 1.4 Å resolution structure of the complex with indole-3-propanole phosphate (IPP), a noncleavable IGP analogue. The interaction of the 3′-hydroxyl of IGP with the catalytic αGlu49 leads to a twisting of the propane chain and to a repositioning of the indole ring compared to IPP. Concomitantly, the catalytic αAsp60 rotates resulting in a translocation of the COMM domain [βGly102-βGly189, for definition see Schneider et al. (1998) *Biochemistry 37,* 5394−5406] in a direction opposite to the one in the IPP complex. This results in loss of the allosteric sodium ion bound at the β-subunit and an opening of the β-active site, thereby making the cofactor pyridoxal 5′-phosphate (PLP) accessible to solvent and thus serine binding. These findings form the structural basis for the information transfer from the α- to the β-subunit and may explain the affinity increase of the β-active site for serine upon IGP binding.

Tryptophan synthase (TRPS,[1] EC 4.2.1.20) is a bifunctional pyridoxal-5′-phosphate (PLP)-dependent tetrameric enzyme—arranged in a linear αββα form—that catalyzes the last two steps in the biosynthesis of L-tryptophan. In the physiologically important "α/β-reaction", indole-3-glycerol phosphate (IGP) and L-serine are condensed to form L-tryptophan and water (for reviews see Figure 1 and (*1*−*4*)). In its α-subunits, the enzyme catalyses the α-reaction (Figure 1), the cleavage of indole-3-glycerol phosphate to indole and glyceraldehyde-3-phosphate (G3P). Subsequently, indole is condensed with serine in a pyridoxal-5′-phosphate mediated reaction at the β-active site (β-reaction). The failure to detect indole even in rapid chemical quench experiments (*5*) and the existence of a ∼25 Å long tunnel that connects the α- and β-active sites (*6*) strongly suggests that indole is transferred through this tunnel from the active site in the α-subunit to the one in the β-subunit (Figure 1). This process, the transfer of an intermediate or metabolite between two sequential enzymes without free diffusion through the solvent is known as substrate channeling. Channeling is thought to play an important role in metabolite regulation and cellular modulation of enzymatic activities and has, therefore, attracted a lot of attention, recently (*1, 7*−*11*). In the case of tryptophan synthase, it prevents loss of the intermediate indole through the cell membranes.

An important requirement for enzymes exhibiting substrate channeling is a tight allosteric regulation of the two coupled reactions so that they remain in phase. In the case of tryptophan synthase, synchronization is achieved first by the influence of the α-site ligand on the affinity for serine and the distribution of the intermediates formed at the β-active site upon binding and subsequent reaction of serine and the PLP cofactor (for review (*2, 3*)). Second, IGP cleavage and transfer of indole through the tunnel is enhanced dramatically upon formation of a highly reactive aminoacrylate intermediate at the β-active site (*5, 12, 13*). This prevents accumulation of indole in the tunnel or at the β-active site as the transfer of indole through the tunnel is fast, and the reaction with the aminoacrylate is largely irreversible. Since the aminoacrylate intermediate is pivotal for the allosteric interaction between the two active sites, we recently determined the crystal structure of TRPS complexed with the aminoacrylate intermediate at the β-active site and the inhibitor 5-fluoroindole-3-propanol phosphate (F-IPP) at the α-site, respectively, under steady-state conditions of the reaction using a flowcell (*14*). The comparison with the structures of TRPS determined in the absence and presence of F-IPP led to the identification of a rigid, but movable domain in the β-subunit. This "COMM-domain", related to the "mobile domain" defined by Rhee et al. (*15*), interacts on the one side with the α-subunit via loop αL2 that interacts with the indole ring of IPP and on the other side with the β-active site. We

* Corresponding author. Telephone: +49 231 133-2738. Fax: +49 231 133-2797. E-mail: ilme.schlichting@mpi-dortmund.mpg.de.

† The beamline X12C is supported by the US Department of Energy Offices of Health and Environmental Research and of Basic Energy Sciences, and by the National Science Foundation. This work was funded by BMBF grant 05SH8EDB1. The atomic coordinates and structure factor amplitudes have been deposited with the Protein Data Bank, Research Collaboratory for Structural Bioinformatics, (http://www.rcsb.org/pdb/). PDB entries (1QOP) for $TRPS^{IGP}$ and (1QOQ) for $TRPS^{IPP}$.

[1] Abbreviations: G3P, glyceraldehyde 3-phosphate; GP, D,L-α-glycerol 3-phosphate; IGP, indole 3-glycerol phosphate; IPP indole propanol phosphate; F−IPP, 5-fluoroindole propanol phosphate; PLP, pyridoxal 5′-phosphate; TRPS, native wild-type tryptophan synthase; $TRPS^{IGP}$, complex of TRPS with IGP; $TRPS^{IPP}$, complex of TRPS with IPP; TRPS-α$D60N^{IPP}_{Ser}$, complex of the TRPS-αD60N mutant with IPP and L-serine.

10.1021/bi9920533 CCC: $18.00
Published on Web 11/25/1999

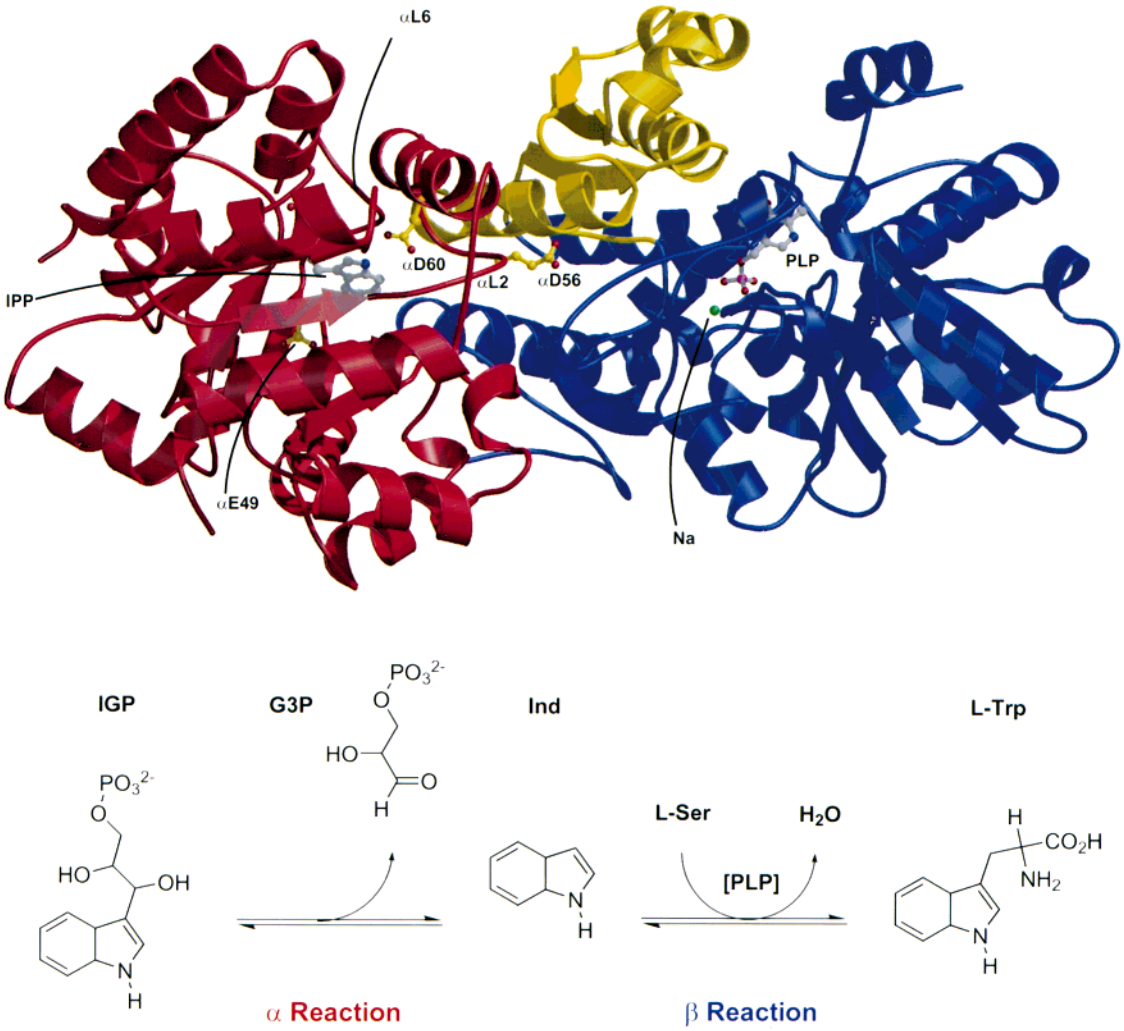

FIGURE 1: Top, schematic representation of the overall fold of the $\alpha\beta$-dimer of TRPS^{IPP}. IPP and PLP bound to the α- and β-subunit, respectively, and the functional important residues αGlu49, αAsp56, and αAsp60 in α-subunit are represented by balls and sticks. The sodium ion is drawn as green ball. Color coding: α-subunit in red, β-subunit in blue, and β-residues belonging to the COMM in yellow. The figure was prepared using "MOLSCRIPT" (*47*) and "RASTER3D" (*48, 49*). Bottom, scheme of the α and β TRPS reaction.

used these findings to propose a detailed structural model for the allosteric communication in TRPS (*14*). Important features of the model that provides a structural explanation for mutagenesis data include the concomitant ordering of loops αL2 and αL6 upon binding of IPP. This results in blockage of the tunnel entrance both directly by αL2 and indirectly by a concerted reorientation of βTyr279 and βPhe280 (*14*, *15*). A central role is taken up by αAsp60, a residue shown to be essential for IGP cleavage (*16*). The αAsp60 carboxylate group not only forms a strong hydrogen bond with the indolyl nitrogen of IPP as required for proton abstraction or ring tautomerization prior to IGP cleavage, but also interacts with the catalytically important αThr183 located in αL6, and with βArg175 located in βH6 of the COMM domain (*14*, *15*). In addition, αAsp60 interacts with and thus positions other residues that link αL2 and αL6 to each other or to the COMM domain in the β-subunit, respectively. Thus, αAsp60 not only plays a crucial role in catalysis of the α-reaction but also in intersubunit communication. This has been also been concluded recently by Rhee et al. (*17*) based on the structure of the TRPS-αD60N$^{IPP}_{Ser}$ complex.

The IPP-induced interactions between αL2 and αL6 of the α-subunit and βH6 located in the COMM domain result in a rigid body movement of the latter. Intradomain interactions transmit the rigid body movement of the COMM domain to βL3, which is located next to the cofactor PLP and contains the catalytically important βGlu109 (*5*, *18*). Another route of transmitting the information on the nature of the α-subunit ligand to the β-active site involves βAsp305. Its orientation is metal dependent (*19*), which may explain the dependence of the catalytic rate on monovalent cations (*20*−*23*).

Most of the results of mutagenesis studies, either performed in a site-directed fashion or by characterization of missence mutations can be rationalized on the basis of the crystal structures of the wild-type and mutant forms of TRPS complexed with either nothing, IPP, F-IPP, or GP at the α-active site and/or nothing, serine, aminoacrylate, or tryptophan at the β-active site, respectively (*14*, *15*, *24*). A notable exception was αGlu49, whose replacement results in inactivation of the α-reaction (*25*); it is believed that αGlu49 abstracts a proton from the C3′-hydroxyl group of the glycerolphosphate moiety of IGP to form glyceraldehyde phosphate (*26*). However, αGlu49 points away from the modeled position of the 3-hydroxyl group of IGP based on the structure of the IPP complex. Recently, Rhee et al. (*27*) determined the crystal structure of the IGP complex of the

Table 1: Crystal Parameters, Data Collection, and Refinement Statistics

	TRPS^{IPP}	TRPS^{IGP}
	crystal parameters	
Unit cell ($a \times b \times c$) [Å]	182.8 × 60.3 × 67.4	182.5 × 60.0 × 67.2
(β) [deg]	94.7	94.5
	data statistics	
resolution [Å]	30.3−1.4	31.2−1.8
no. of observations	294137	219018
no. of unique reflections	143761	63674
completeness (total/high) [Å][a]	93.2/80.8	94.5/70.8
R_{sym} (total/high)[b]	5.7/25.8	7.6/20.9
$\langle I/\sigma(I)\rangle$ (total/high)	10.3/2.4	11.7/2.6
	refinement statistics	
resolution range [Å]	20.0−1.4	20.0−1.8
included amino acids	α1−α190, α193−α267, β2−β391	α1−α178, α193−α268, β2−α396
Φ/Ψ-torsion angle validation; only non-glycine and non-proline residues	αF212	αF212
no. of protein atoms	4952	4898
no. of waters	801	516
no. of ligand atoms	32	34
no. of metal ions	1	0
R_{work}, R_{free}[c] [%]	15.0/17.7	17.1/21.0
rmsd bonds/angles [Å/deg]	0.012/1.4	0.017/1.3
$\langle B\rangle$ (mc/sc/lig/wat) [Å^2]	14.6/18.3/12.8/31.0	18.3/21.5/17.3/33.4
alternative side chain conformations/*: alternative backbone conformations	αI30, αE31, αE90, αC154, αP156*, αN157*, αA158*, αS178, αE254 βE11, βM22, βS34, βK37, βK50, βK61, βI65, βM152, βT165, βK219, βM240, βH260, βR341, βE367, βR379	αE49, βC170, βE182, βM240

[a] Completeness, R_{sym} and $\langle I/\sigma(I)\rangle$ are given for all data and for the highest resolution shell: TRPS^{IPP} 1.5−1.4 Å, TRPS^{IGP} 1.9−1.8 Å. [b] $R_{sym} = \sum|I-\langle I\rangle|/\sum I$. [c] $R_{work} = \sum|F_{obs}| - k|F_{calc}|/\sum|F_{obs}|$. 5% of randomly chosen reflections were used for R_{free}.

catalytically impaired αD60N mutant, using a cryo-crystallographic approach. In this structure, αGlu49 does indeed interact with the C3′-hydroxyl group of IGP as proposed for the reaction mechanism of the α-reaction mentioned above.

Despite the success of finally seeing this proposed interaction in the TRPS-αD60N^{IGP} complex there are limitations in the implications on the enzymatic mechanism of this structure. Unfortunately, αAsp60 not only has a catalytic role but is also central to intersubunit communication as described above. To obtain information on the roles of αGlu49 and αAsp60 in the catalytic mechanism of the α-reaction and the α/β subunit communication, we determined the crystal structures of wild-type TRPS complexed to the α-substrate IGP and the α-substrate analogue IPP to 1.8 and 1.4 Å resolution, respectively. We show how the binding of IGP at the α-active site induces via αAsp60, a large displacement of the COMM domain that results in loss of the Na^+ ion and an opening of the β-active site. The implications for the catalytic mechanism of TRPS are discussed.

MATERIALS AND METHODS

Crystallization and Substrate−Complex Preparation. Native wild-type TRPS was expressed and purified as described (*28*). The protein was stored at a concentration of 10 mg/mL in a solution containing 50 mM bicine pH 7.8, 10 mM Na-EDTA, 1 mM di-thioerythritol and 20 μM PLP. Crystals were grown in the dark at room temperature using the hanging drop method by mixing equal volumes (3−5 μl) of protein and reservoir solutions. The latter contained 50 mM bicine buffer pH 7.8, 5 mM di-thioerythritol, 5 mM Na-EDTA, 0.1 mM PLP, 2 mM spermine, 2 mM NaN_3 and 8−12% (w/v) PEG 8000. The substrate IGP was prepared enzymatically from indole and G3P by the reverse α-reaction of TRPS (*29*); the substrate analogue IPP was a generous gift of Karen Anderson. The TRPS^{IPP} complex was obtained by cocrystallization using an initial IPP concentration of 7 mM in the crystallization droplet. Prior to flash-freezing in liquid nitrogen the crystals were rinsed briefly in a cryo-protectant solution consisting of 100 mM Na-HEPES pH 7.8, 15% (w/v) PEG 8000, and 20% (v/v) glycerol. The TRPS^{IGP} complex was generated by soaking native wild-type TRPS crystals for 2 min in the cryo-protectant solution containing 23 mM IGP before flash-freezing in liquid nitrogen.

X-ray Data Collection. Diffraction data of the TRPS^{IGP} complex were collected at beamline X12c at the NSLS using a wavelength of 1.0 Å and the Brandeis 2K × 2K CCD detector. Data of the TRPS^{IPP} complex were collected at beamline X11 at EMBL c/o DESY using a wavelength of 0.9076 Å and a MAR345 detector. All measurements were carried out at 100 K. The diffraction data were processed with XDS and scaled with XSCALE (*30*). Data statistics are given in Table 1.

Refinement. The coordinates of native wild-type TRPS (PDB accession code 2WSY) (*14*) were used as a starting model for the TRPS^{IPP} refinement. After completing the refinement of TRPS^{IPP} at a maximum resolution of 1.4 Å, this final model was used as starting model for the TRPS^{IGP} refinement. In both cases, water molecules, the PLP cofactor, and the α-subunit ligand IPP were omitted and an overall *B*-factor of 20.0 Å^2 was assigned. In general, the same refinement strategy was applied for both enzyme complexes using protocols and programs of the CNS 0.4 (*31*) and the CCP4 suite (*32*). Manual rebuilding and map interpretation by inspection of SigmaA-weighted $2mF_{obs}-DF_{calc}$ (*33*), $3F_{obs}-2F_{calc}$, and SigmaA-weighted $mF_{obs}-DF_{calc}$ (*33*) difference electron density maps was done with the graphics program "*O*" (*34*). After an initial rigid-body refinement cycle of both TRPS subunits, possible model bias was

removed by two cycles of simulated-annealing using the slow-cooling protocol at a starting temperature of 2500 K (*35*); a bulk-solvent correction was introduced in the second cycle. Subsequently, the geometrically restrained refinement was carried on using "PROTIN/REFMAC" (*33*). Ideal bond lengths and angles for IGP, IPP, and the cofactor PLP, respectively, were derived from the following PDB entries: IGP coordinates were taken from PDB entry 1A5B (*27*), IPP from 2TRS (*15*), and PLP from 2WSY (*14*). Clear electron density was visible even after the initial rigid-body refinement step for the ligand molecules IGP, IPP, and the covalently bound PLP-cofactor. Thus, they were added to the atomic model since the first rounds of maximum likelyhood-refinement. Solvent molecules were incorporated automatically using the program "ARP" (*37*). All water molecules were checked manually and removed from the model if they did not have at least one hydrogen binding partner. During the final refinement stages of both complexes, additional electron density for several amino acid side chains appeared and a second side-chain conformation was introduced for these residues in both models. The atom occupancies were checked manually by adjusting the *B*-factors to the same level for both conformations. A list of residues with double conformations is given in Table 1.

In case of TRPS^{IPP}, careful inspection of a SigmaA-weighted $mF_{obs} - DF_{calc}$ electron density map of the final model at 1.4 Å resolution showed additional electron density for side chain atoms of several buried amino acid residues. This density was attributed to an anisotropic atom vibration. Therefore, anisotropic *B*-factors were introduced in the last steps of the TRPS^{IPP} refinement. Refinement statistics for both enzyme complexes are given in Table 1.

Structure Superposition. To investigate the influence of different ligands of the α-active site on the allosteric communication, we superimposed other TRPS structures on the TRPS^{IPP} coordinates, which represent the TRPS structure with highest resolution presently available. The superposition was done with the program "O" (*34*) using all common C_α-atom coordinates of both structures, except the C_α atoms belonging to the COMM domain (βGly102-βGly189, (*14*)). The resulting RMS deviations were calculated with the program "BRAGI" (*38*).

RESULTS

Model Quality and Structure Description. The structural models of the IPP and IGP complexes of TRPS are of high quality as indicated by the low crystallographic validation values and the small mean deviations of the geometrical parameters from their ideal values (Table 1). Both TRPS complex structures share the same secondary and tertiary structure, and the overall topology is similar to the one assigned by Schneider et al. (*14*). Larger backbone differences between TRPS^{IGP} and TRPS^{IPP} exist only in the region of the loops αL2 and αL6, and in the COMM domain. The nature and the origin of these differences will be discussed in the following sections in more detail.

No clear electron density was found for the loop αL6 residues αAla190 and αLeu191 in case of TRPS^{IPP}, and αArg179 to αPhe192 in TRPS^{IGP}, respectively. Also, the C-terminal residue αAla268 and those downstream of βLys392 in case of TRPS^{IPP} are not included in the final model as are the ones C-terminal of βGlu395 in TRPS^{IGP}. Furthermore, some solvent accessible residues exhibit very weak or poor side-chain electron density, but all atoms were included in the refinement. Exceptions were made for amino acid side chains shown or proposed to play either an important role in the intersubunit communication (*14*) or catalysis. Therefore, βArg175 located in the helix βH6 was modeled as alanine in TRPS^{IGP}.

In both structures, all amino acids, except αPhe212, exhibit allowed ϕ/ψ-torsion angle pairs in the Ramachandran plot. This is in agreement with all TRPS structures complexed with indole derivatives at the α-site (*6*, *14*, *15*): closure of loop αL6 causes a hydrophobic interaction of the αPhe212 phenol ring and the indole moiety of the α-ligand, which may compensate for the unfavorable backbone conformation. This interaction is also found in TRPS^{IPP}. In TRPS^{IGP}, the higher flexibility of loop αL6 results in weak electron density for the αPhe212 side chain. However, careful inspection of a SigmaA weighted $mF_o - DF_c$ difference map (*33*) shows a more open conformation for the αPhe212 side chain, which does not form the aforementioned interaction with the indole ring of IGP.

The 1.4 Å resolution of the diffraction data and the excellent quality of the model of the TRPS^{IPP} complex (see Table 1) allows analysis of the atomic hybridization states. Of particular interest is the geometry of the Schiff base linkage between the amino group of lysine βLys87 and C_{4A} of the PLP cofactor at the β-active site. Interestingly, this bond appeared nonplanar in the 1.4 Å resolution TRPS^{IPP} structure. We tested different strong bond restraints in the refinement for keeping the internal aldimine planar. However, the resulting models, difference electron density maps, and omit maps calculated without PLP and the lysine side chain, respectively, were only consistent with a nonplanar C_{4A}-N_ζ bond (see Figure 5). Therefore, no special bond restraints for the Schiff base linkage between PLP and βLys87 were applied.

IPP Binding. The coordinates of the structure of the IPP complex of wild-type TRPS (*6*) are not deposited in the PDB. Therefore, we redetermined the structure of this complex. The exceptionally high resolution (1.4 Å) and quality of the TRPS^{IPP} structure allows us to describe the IPP-binding mode with great detail and unprecedented precision (see Figure 2A). The IPP-binding mode is essentially the same as in the TRPS-βK87T^{IPP} (*15*) and the TRPS^{F-IPP} complex (*14*). This supports our previous assumption that the fluorine atom does not influence the F-IPP binding mode.

The phosphate group is positioned above the N-terminal side of α-helix αH8′, thereby interacting with the positive helix dipole moment. Compared to the ligand-free wild-type TRPS structure (PDB accession code 1WSY (*6*) and 2WSY (*14*)) IPP binding induces stabilization of loop αL2 residues[2] and closure of loop αL6. This agrees with our previous observation on the TRPS^{F-IPP} complex (*14*) but disagrees

[2] Recently a structural model of a ligand free wild-type structure refined to higher resolution (2.2 Å, PDB accession code 1BKS (*24*)) became available that includes also coordinates for loop αL2 residues. However, the average temperature factor for these atoms is approximately 1.5 times higher than the average value for all atoms, pointing to the very mobile nature of loop αL2. Unfortunately, the coordinate set does not contain crystallographic validation and statistical parameters that would allow to assess the quality of the model.

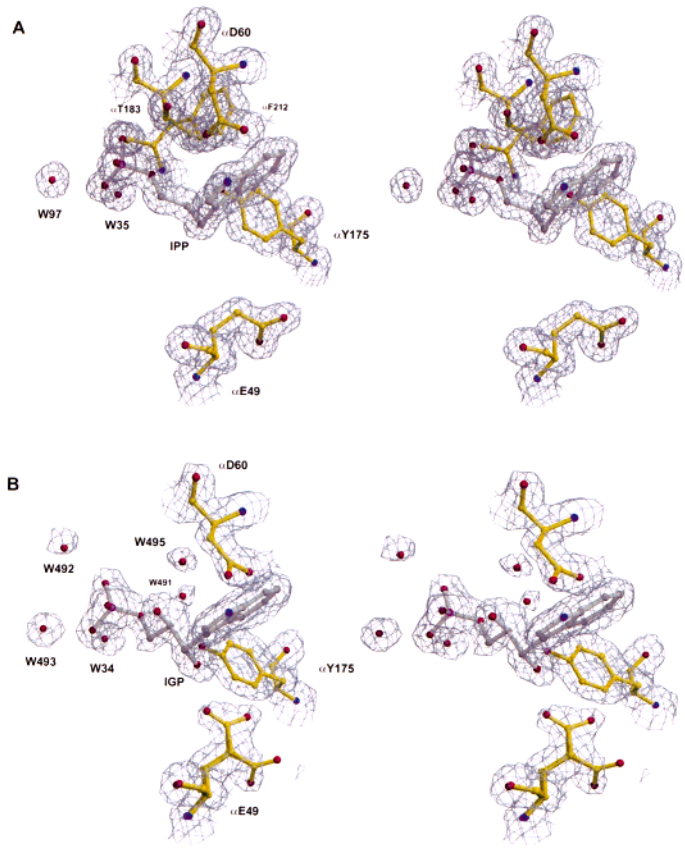

FIGURE 2: Stereo drawing of SigmaA-weighted $2mF_o-DF_c$ maps contoured at 1σ around the α-active site showing the binding of IPP (A) and IGP (B) in wild-type TRPS. Oxygen atoms are colored in red, nitrogen in blue, phosphate in magenta, protein carbon atoms in yellow and ligand carbon atoms in gray. The figure was prepared using "BOBSCRIPT" (*50*) and "RASTER3D" (*48*, *49*).

with findings by Hyde et al. (*6*) on the TRPS^{IPP} complex and conclusions by Rhee et al. (*15*).

The IPP molecule forms a number of electrostatic interactions with different parts of the enzyme; the phosphate forms hydrogen bonds with the hydroxyl (2.6 Å) and the amide nitrogen atom (2.7 Å) of αSer235 via oxygen O_{P1}, with the amide of αGly234 (2.9 Å) and two water molecules (W35, 2.6 Å; W97, 3.0 Å) via O_{P2} and with the amide nitrogen atoms of αGly184 (2.9 Å) and αGly213 (2.8 Å) via O_{P3}. The indole nitrogen atom forms a hydrogen bond with αAsp60−$O_{\delta 1}$ (2.9 Å). The aromatic indole ring forms hydrophobic contacts with the side chains of αPhe22, αIle64, αLeu100, αTyr102, αLeu127, αIle153, and αTyr175. The propane chain interacts with αThr183 and αIle232. As in the TRPS^{F-IPP} and TRPS-βK87T^{IPP} structures the side chain of αPhe212 is positioned perpendicular to the indole ring, which seems to be a prerequisite for the closure of loop αL6.

The side chains of the catalytic residues αGlu49 and αAsp60 (*16*, *26*, *39*, *40*) adopt the same conformation as in the TRPS-βK87T^{IPP} and TRPS^{F-IPP} complexes: the oxygen atom $O_{\delta 1}$ of the carboxylate group of αAsp60 hydrogen bonds with the indole nitrogen atom N_1 (2.9 Å) and with αThr183-$O_{\gamma 1}$ (2.8 Å), thereby positioning loop αL6. The side chain of αGlu49, assumed to be involved in proton transfer from the glycerol phosphate moiety to the indole ring (*16*) is pointing away from the scissile C3−C3′ bond in the IPP complex.

IGP Binding. Microspectrophotometric studies on microcrystalline slurries (*41*) and single crystals (*42*) of TRPS have shown that the active sites of both the α- and the β-subunit are functional in the crystalline state although with changed K_m and K_I values for some inhibitors and with somewhat reduced rates. This allows to generate the TRPS^{IGP} substrate complex by diffusing IGP in the crystals with subsequent freeze trapping. Indeed, strong electron density for IGP was visible from the very start of the refinement and allowed to place the molecule unambiguously. Since αGlu49 only adopts the extended side chain conformation upon IGP binding to the α-active site, the IGP occupancy was set to the same value as found for the extended αGlu49 conformation (80%). This restraint led to an average IGP temperature factor of 24.0 Å^2.

Interestingly, the binding modes of IGP and IPP differ remarkably (Figure 2). Although the IGP phosphate group binds at an identical position at the N-terminal side of the helix αH8′, there is no electron density for loop αL6 in the TRPS^{IGP} complex. Because of this missing loop the hydrogen bonding network of the phosphate oxygen atoms is slightly different: as in the IPP complex the oxygen atom O_{P1} hydrogen bonds with the hydroxyl (2.7 Å) and the amide nitrogen atom (2.6 Å) of αSer235; oxygen atom O_{P2} hydrogen bonds with the amide nitrogen atom of αGly234 (2.7 Å) and two water molecules (W34, 2.7 Å; W88, 2.6 Å); oxygen atom O_{P3} interacts with the amide nitrogen atom of αGly213 (2.8 Å) and with water W492 (2.9 Å), and the bridging oxygen atom O_{P4} forms a hydrogen bond to water molecule W491 (2.9 Å). These two latter water molecules are replaced by loop αL6 in TRPS^{IPP}.

As shown in Figure 2B, the two additional hydroxyl groups at the C2′ and C3′ atoms of IGP form hydrogen bonds to

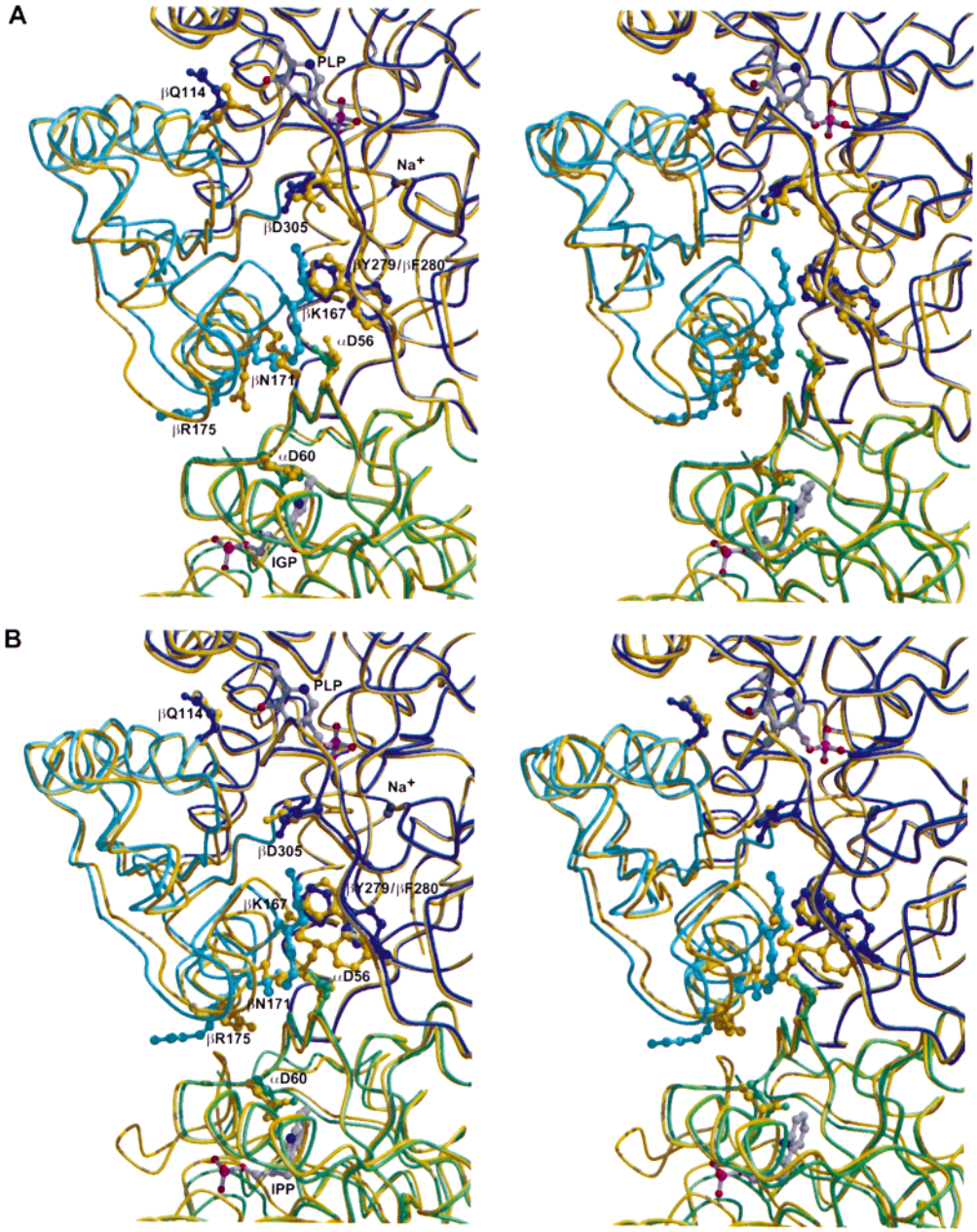

FIGURE 3: Stereoview of the TRPS structure superposition focused on the COMM domain. C_α trace of ligand free TRPS/TRPS^{IGP} (A) and ligand free TRPS/TRPS^{IPP} (B). Some residues with assigned function in catalysis or communication are shown in ball-and-stick representation. C_α traces and residues of ligand free TRPS are colored in green (α-subunit), dark blue (*β*-subunit) and light blue (COMM domain), TRPS^{IGP} (A) and TRPS^{IPP} (B) in yellow, α-ligands and cofactor PLP carbon atoms are colored in gray, oxygen in red, nitrogen in blue and phosphate in magenta, Na^+ ions in dark brown (ligand free TRPS) and light brown (TRPS^{IPP}). The figure was prepared using "MOLSCRIPT" (*47*) and "RASTER3D" (*48, 49*).

water molecule W495 (2.9 Å), to αTyr175-O_ζ (2.8 Å), and to αGlu49-$O_{\epsilon 1}$ (2.5 Å), respectively. The latter interaction is also observed in the TRPS-αD60N^{IGP} mutant complex (*27*) and supports the proposed catalytic role of αGlu49, which is believed to attack the hydroxyl group on C3′.

These additional hydrogen bonds cause a different torsion angle around the C2′−C3′ bond of 171° for IGP compared to 82° for IPP. The anchoring of the substituted propane chain induces a rotation of ∼21.7° and thus a reorientation of the indole ring (Figure 3A). This results in an indole nitrogen movement of 0.9 Å toward the side chain of the second catalytic residue αAsp60. In combination with the missing closure of loop αL6 this indole movement induces a shift of the backbone of the αL2 amino acids αAsp56 to αAsp60 in TRPS^{IGP}, culminating in a 1.0 Å translation and a ∼40° rotation of the carboxylate group of αAsp56. This shift of the αL2 residues alters the entire hydrogen network properties of loop αL2, which is a crucial part of the α/*β* subunit interface.

As a consequence of the loop movement, the well defined hydrogen bonds in the TRPS^{IPP} complex from *β*Lys167 (2.8 Å) and *β*Asn171 (2.7 Å) to αAsp56, and from *β*Arg175 to αPro57 (2.9 Å) and αAsp60 (2.9 Å) are broken in case of TRPS^{IGP} and a new set of hydrogen bonds is established; in TRPS^{IGP} *β*Lys167 forms a hydrogen bond to αSer55-O_γ (2.9 Å), *β*Asn171 to αAsp60 O (2.8 Å), and αGln65-N $_{\delta 2}$ (2.8 Å). In addition, the link of the COMM domain residues *β*Lys167 (3.0 Å) and *β*Asn171 (2.8 Å) to the "gating residue"

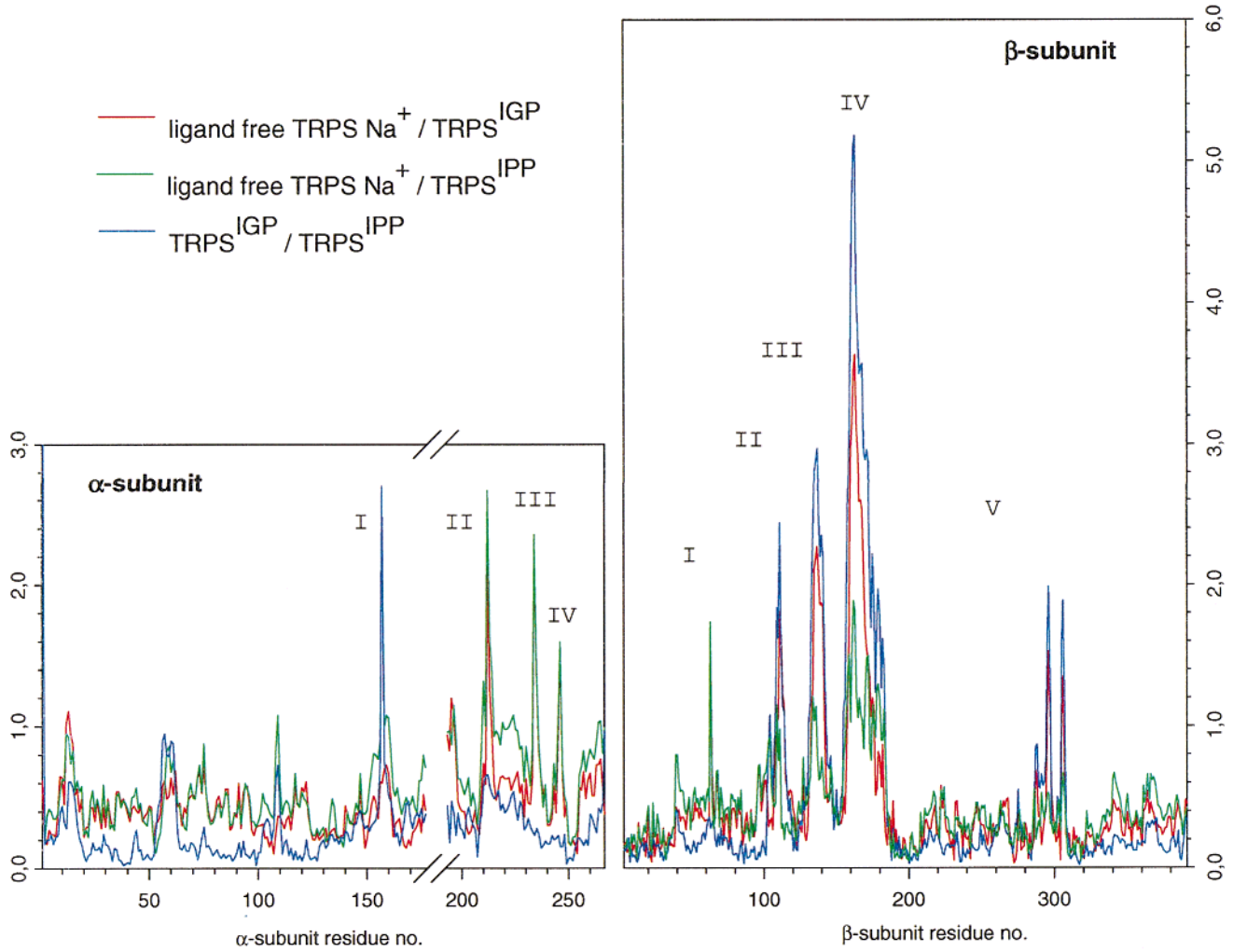

FIGURE 4: C_α rms deviation of TRPS^{IGP}, TRPS^{IPP}, and ligand-free TRPS (*24*) for the TRPS α (left) and *β* (right) subunits. Points I_α, IV_α, and V_β represent flexible surface residues. Points II_α and III_α represent C_α deviations of ligand-free TRPS αPhe212 and αGly234, which adopt several conformations involved in α-site ligand binding. Points II_β to IV_β show the large COMM domain rigid body movement upon ligand binding.

*β*Tyr279 that is observed in the TRPS^{IPP} structure is missing in TRPS^{IGP} and the *β*Tyr279 side chain adopts an "open channel" conformation.

COMM Domain Movement. Because of the altered hydrogen bonding pattern of loop αL2 in the TRPS^{IGP} complex, a remarkable rigid-body movement of the COMM domain relative to its position in the IPP complexed and the ligand-free wild-type TRPS takes place (see Figures 3 and 4). The largest displacement occurs at the N-terminal side of helix *β*H6 (*β*Thr165−*β*Tyr181) and the preceding loop *β*L5 (*β*His160−*β*Ala164) and sheet *β*S5 (*β*Glu155−*β*Val159), at the N-terminal part of helix *β*H5 (*β*Ile132−*β*Ser143), including the C-terminal part of loop *β*L4, and at the region around loop *β*L3 (*β*Ala108−*β*His115), that contains catalytically important residues for the *β*-reaction. The maximal C_α atom movement is found at residue *β*Ser163 with a shift of 5.2 Å. Within the COMM domain, all secondary structure elements, which have contacts to the α-subunit, moved away from the core of the *β*-subunit, leading to an open TRPS^{IGP} enzyme complex at the *β*-active site.

The opening of the TRPS enzyme upon IGP binding at the α-site is in contrast to findings in all published IPP/F-IPP wild-type structures (TRPS^{IPP}, TRPS^{F-IPP} (*14*), TRPS-*β*K87T^{IPP} (*15*)) and also to the TRPS-αD60N^{IGP} (*27*) and TRPS-αD60N$^{IPP}_{Ser}$ structures (*17*); comparisons of the IPP complexed TRPS structures with ligand-free ones show that upon binding of IPP to the α-subunit, the COMM domain moves toward the *β*-subunit core. This is the opposite direction compared to the movement upon IGP binding. The observation of an open TRPS^{IGP} complex agrees with results from kinetic experiments reporting a high affinity of the active site of the *β*-subunit for L-serine upon binding of IGP to the α-subunit (*12*).

Metal Binding. The TRPS^{IPP} and TRPS^{IGP} complexes were both obtained in the presence of sodium ions. In the TRPS^{IPP} complex, the coordination of the sodium ion is tetragonal pyramidal, with the planar ligands formed by the carbonyl oxygen atoms of *β*Phe306, *β*Ser308 and two water molecules, and the apical ligand formed by the carbonyl oxygen atom of *β*Gly232, respectively (Figure 5A). The coordination geometry is very similar to the one observed for the ligand-free TRPS (PDB entry 1BKS (*24*)). It is, therefore, extremely surprising that the sodium ion is missing in the TRPS^{IGP} complex (Figure 5B). This is caused by the large IGP induced COMM domain movement described in detail above. This movement disrupts the hydrogen bonding network that links several residues of the COMM domain to residues involved

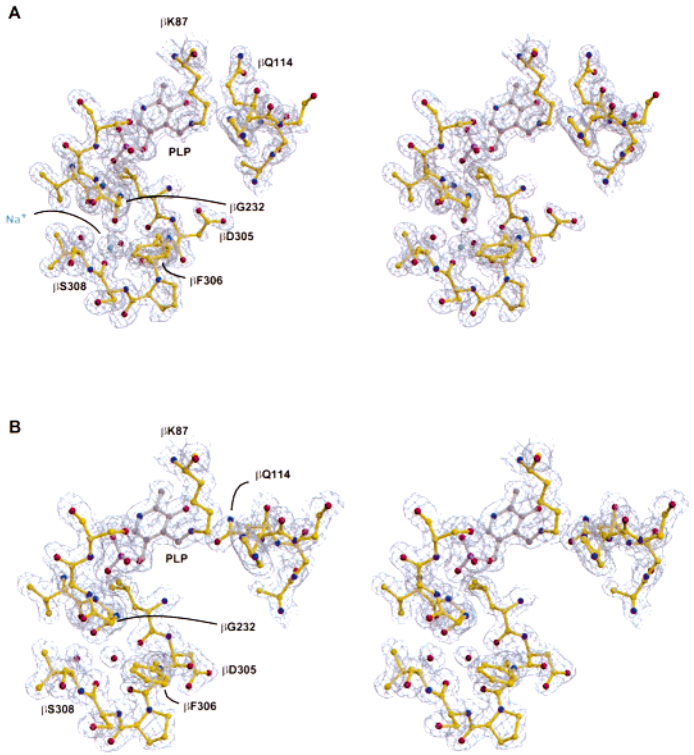

FIGURE 5: Stereo drawing of SigmaA-weighted $2mF_o-DF_c$ maps contoured at 1σ level around the sodium binding site, βAsn114, and the prosthetic PLP group of TRPS^{IPP} (A) and TRPS^{IGP} (B). Oxygen atoms are colored in red, nitrogen in blue, phosphate in magenta, sodium in light blue, protein carbon atoms in yellow and ligand carbon atoms in gray. The figure was prepared using "BOBSCRIPT" (*50*) and "RASTER3D" (*48, 49*).

in ion binding or that are located nearby; in the TRPS^{IPP} complex, the COMM domain residues βAsp138, βGln142, βThr165, and βLys167 are linked via one or two water molecules, respectively, to βAsp305 involved in sodium coordination. The second hydrogen bonding network connects the βSer163 carbonyl oxygen atom (2.9 Å) and the βLys137 N_ζ nitrogen (2.8 Å) via a water molecule (2.8 Å) to βGlu296. The neighboring βThr297 O_γ oxygen forms a direct hydrogen bond to the carbonyl oxygen of βPhe306, involved in ion binding. All water molecules exhibit very well-defined electron density and have temperature factors lower than 41 Å^2 (mean value 29.2 Å^2). This hydrogen bonding network is disrupted upon the IGP-induced COMM domain movement. The consequent liberation of the βAps305 side chain entails a C_α-backbone atom shift of residues βAsp305 and βPhe306 by more than 1.5 Å. This backbone movement includes the carbonyl oxygen atoms of βAsp305 and βPhe306 and results in a narrowing of the metal binding loop "squeezing" out the sodium ion. Interestingly, careful inspection of the final TRPS^{IPP} electron density showed residual electron density for residues of both aforementioned β-loops. This density would agree with backbone traces nearly identical to the ones observed in TRPS^{IGP}, indicating an equilibrium between the two positions of the "cation binding" loops.

DISCUSSION

We investigated the structural and functional role of the catalytically important amino acid residues αGlu49 and αAsp60 of the tryptophan synthase α-subunit. Both residues have an assigned function in the cleavage of indole-3-glycerol phosphate in the α-subunit and in the allosteric communication between the α- and β-subunits of the tryptophan synthase bienzyme, respectively. This subunit interaction is influenced by pH, temperature, monovalent cations, and especially, by the active site ligands. We used freeze trapping to stabilize the wild-type tryptophan synthase indole-3-glycerol phosphate Michaelis complex and determined its structure to 1.8 Å resolution. In addition, we determined the 1.4 Å resolution structure of tryptophan synthase complexed with IPP, a noncleavable IGP analogue that lacks the hydroxyl groups at the 2′ and 3′ positions of the propane chain.

Both TRPS complexes have the same topology as the other TRPS structures although minor differences in the secondary structure definition as established by DSSP (*43*) are observed. Despite the similarity of the two α-active site ligands IGP and IPP, rigid body movements of the COMM domain in opposite directions relative to unligated TRPS (*24*) take place in TRPS^{IGP} and TRPS^{IPP} complexes (Figure 4). The TRPS^{IGP} structure shows the largest rigid-body movement of the COMM domain observed so far, which results in an opening of the TRPS β-subunit. Since this opening is induced only upon binding of IGP and not of IPP or F-IPP (*14*), the introduction of the two hydroxyl groups at the C2′- and C3′-carbon atoms of the propane side chain of IGP and their interactions with the enzyme has to officiate as the origin for the opposite rigid-body COMM domain movement as described in detail below.

The structures of the TRPS^{IGP} and TRPS^{IPP} complexes confirm the observation of a loop αL2 stabilization upon ligand binding at the α-site (*14, 15*). Loop αL2 is involved in the intersubunit communication through a hydrogen bonding network to residues of the βH6 helix located in the COMM domain. In case of TRPS^{IPP}, loop αL6 is also closed

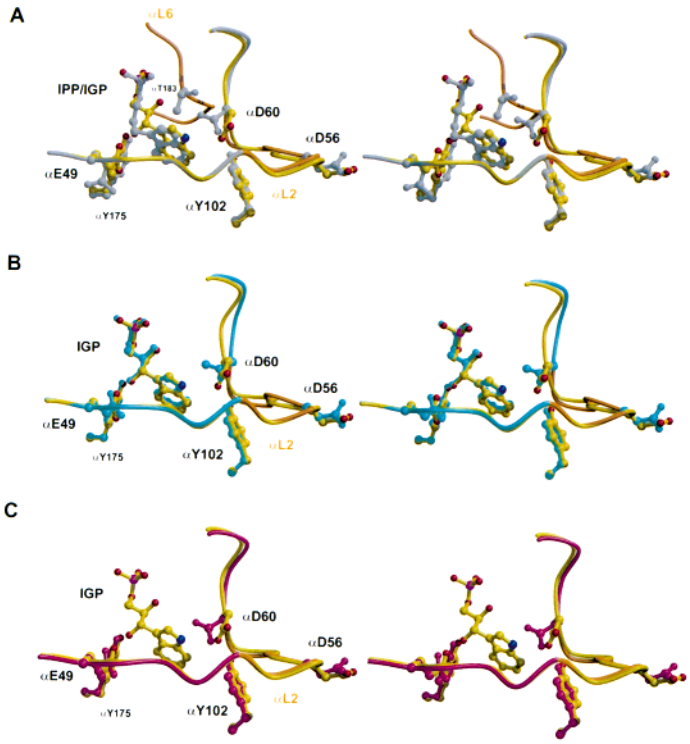

FIGURE 6: Stereoviews of TRPS structure superpositions at the α-active site. $TRPS^{IGP}$ coordinates (in yellow) are superimposed with (A) $TRPS^{IPP}$ (B) TRPS-αD60N^{IGP} and (C) ligand-free TRPS by using all common C_α-atom pairs, excluding the COMM (*β*Gly102−*β*Gly189) domain residues. Substrate ligands and amino acid residues with special functions in catalysis or allosteric communication are shown in ball-and-stick representation. The figure was prepared using "MOLSCRIPT" (*47*) and "RASTER3D" (*48*, *49*).

as observed previously for the $TRPS^{F-IPP}$ complex (*14*). In contrast, in the $TRPS^{IGP}$ complex the loop αL6 is not visible.

The opposite COMM domain movement in both TRPS complexes is caused by the different hydrogen bonding pattern of loop αL2, which is a consequence of the different binding modes of IGP and IPP (Figure 6A). The IGP reorientation is caused by the interactions of the C3′-hydroxyl group, that forms two well defined hydrogen bonds to both the catalytic α-site residue αGlu49 and the hydroxyl group of αTyr175 resulting in a different torsion angle around the C2′−C3′ bond. As a consequence, the IGP indole ring atoms shift on average by ∼0.7 Å (indole nitrogen by 0.9 Å) toward the αAsp60 side chain. Concomitantly, the carboxylate C_γ atom of this catalytically important residue moves by 1.7 Å and the C_α atom shifts by 0.6 Å relative to the unligated structure. Furthermore, the αAsp60 carboxylate group rotates around the torsion angle χ_1 by ∼45° and around χ_2 by ∼70°. These large side chain and backbone alterations are not observed upon IPP binding. In the $TRPS^{IPP}$ complex, the αAsp60 C*γ* atom moves only by 0.7 Å relative to the ligand free TRPS. The change of the αAsp60 position is transmitted and amplified by backbone and side chain atom shifts of loop αL2 residues resulting in a shift of ∼1.0 Å of the αAsp56 side chain in the $TRPS^{IGP}$ complex. αAsp56 is part of the intersubunit interface and forms two hydrogen bonds to the COMM domain residues *β*Lys167 and *β*Asn171 in the $TRPS^{IPP}$ complex. The movement of αAsp56 in the $TRPS^{IGP}$ complex results in an altered hydrogen bonding pattern; instead of *β*Lys167 and *β*Asn171, the αSer55 carbonyl oxygen and αGln65-$N_{\epsilon 2}$ nitrogen atom hydrogen bond to αAsp56. This new hydrogen bonding network is the reason for the COMM domain displacement resulting in an open *β*-subunit in the $TRPS^{IGP}$ structure (see Figure 7).

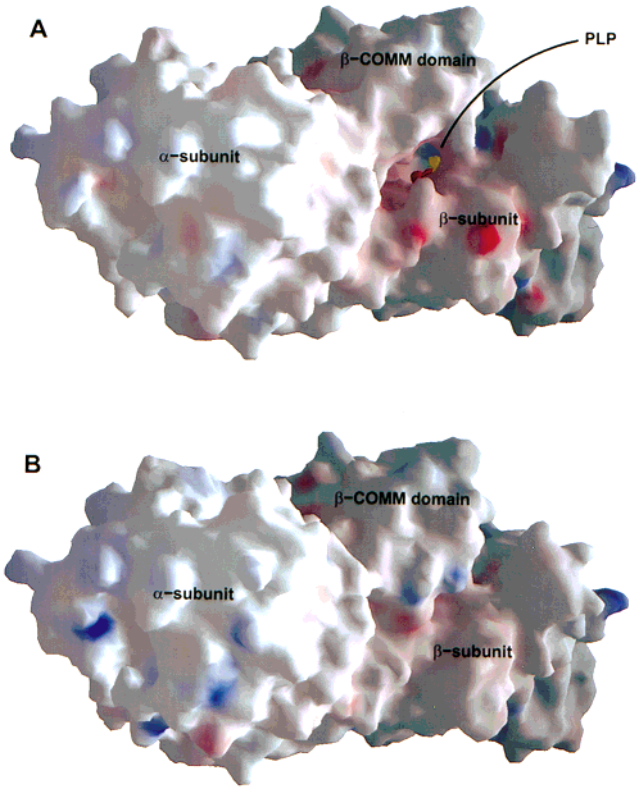

FIGURE 7: Electrostatic surface potential (using the program *GRASP*; (*51*)) of $TRPS^{IGP}$ (A) and $TRPS^{IPP}$ (B) (red, negative; blue, positive; white, uncharged) viewed toward the *β*-active site. The PLP molecule is shown in space filling representation, with oxygen atoms colored in red and carbon in yellow.

In the structure of the IGP complex of the αD60N mutant, which has no measurable activity in the α-reaction but retains

substantial β-subunit activity (*16*), the IGP binding mode is very similar to the wild-type enzyme, and the catalytic αGlu49 adopts the same extended conformation to form a hydrogen bond with the C3′-hydroxyl group (Figure 6B). Interestingly, neither a large COMM domain movement relative to the ligand-free wild-type or the αD60N mutant structure (*24*, *27*) nor a "β-subunit opening" is observed. After the C_α-atom superposition (see Methods) of both IGP complexes, the root-mean-square deviations for all 19 oxygen, nitrogen, carbon, and phosphor atoms of IGP amounts to 0.4 Å.

In contrast to our findings for the wild-type $TRPS^{IGP}$ complex, αAsn60 does not move and the side chain does not rotate in the TRPS-$\alpha D60N^{IGP}$ structure (*27*) (Figure 6B). The mutated asparagine side chain shows the same hydrogen bonding pattern for the oxygen $O_{\delta 1}$ but forms no equivalent hydrogen bond to the IGP indole nitrogen atom via oxygen $O_{\delta 2}$ as in the wild-type structure, since it lacks this oxygen atom. Instead, the side chain nitrogen atom $N_{\delta 2}$ is close to the indole nitrogen (3.1 Å) and to carbon atom $C_{\gamma 2}$ of αIle64 (3.2 Å), respectively. These unfavorable interactions and the missing hydrogen bonding capacity of αAsn60 may be the reason for the surprisingly high-temperature factors (considering the presence of an α-site ligand) for the αL2 residues (αAsp56 to αPro62) in the $\alpha D60N^{IGP}$ complex. Therefore, we believe that the structural differences between the $TRPS^{IGP}$ and TRPS-$\alpha D60N^{IGP}$ complexes concerning the COMM domain movement root in the modified hydrogen bonding property of the mutated aspartate. This emphasizes the importance of αAsp60 not only in the enzymatic IGP cleavage in the α-reaction but also in the intersubunit communication pathway. Although this role for αAsp60 has been deduced by Rhee et al. (*17*) based on the TRPS-$\alpha D60N^{IPP}_{Ser}$ complex, the structure of the mutant does not allow to deduce the interactions in the wild-type enzyme reported here due to the intricate network of interactions that rapidly amplify the magnitude of the conformational changes from the α−β interface to the β-active site.

As mentioned above, loop αL6 is closed in the IPP complex but not in the IGP complex. An obvious reason for the missing αL6 loop closure in case of $TRPS^{IGP}$ is the rigid body movement of the COMM domain away from the β-subunit core, leading to a steric hindrance of loop αL6. The flexible side chain of $TRPS^{IGP}$ βArg175, which is not included in the final model, would be the main reason for preventing the loop closure in $TRPS^{IGP}$. Assuming a similar conformation of the closed loop αL6 in the $TRPS^{IGP}$ and $TRPS^{IPP}$ structures and a sterically allowed side chain conformation of βArg175, the side chain would clash with the closed loop. Thus, it seems that this side chain acts as a molecular "door stop", preventing a premature closure of the active site by loop αL6 with subsequent IGP cleavage before the reactive aminoacrylate is formed at the β-active site. Considering the high quality of our crystallographic data (see Table 1), the observed side chain flexibility of βArg175 is also an indication for the lack of suitable side chain interactions in the open COMM domain state.

However, this finding alone cannot explain why loop αL6 is not closed in the TRPS-$\alpha D60N^{IGP}$ structure, since this complex has no open COMM domain. Inspection of the α-active site of the $TRSP^{IPP}$ complex shows a second sterically problematic interaction of loop αL6, namely the hydrogen bond (2.8 Å) of αThr183 with the αAsp60 side chain. In the $TRPS^{IGP}$ structure, this interaction is no longer possible: first, the carboxylate group of αAsp60 rotated and, therefore, cannot interact with the αThr183 $O_{\gamma 1}$ oxygen; second, the αThr183 carbon atom $C_{\gamma 2}$ as positioned in a closed loop αL6 would be located only 2.2 Å from the IGP C2′-hydroxyl oxygen atom.

Cation Binding Site: *Loss of the Sodium Ion upon IGP Binding*. It was shown by Dunn and co-workers (*20*, *21*) and others (*19*, *23*, *44*) that monovalent cations (Na^+, K^+, Cs^+, NH_4^+) are important effectors of the enzymatic properties of TRPS. Structures of unligated wild-type TRPS−cation complexes have been determined for sodium (*24*), potassium (*19*), and cesium (*19*) ions, respectively. In these structures, a single monovalent cation binding site is observed, which is located approximately 8 Å from the phosphate moiety of the pyridoxal phosphate cofactor. In all three complexes, the cation is coordinated with three to six carbonyl oxygens and one or two water molecules, respectively. The coordinating residues common in all three complexes are βPhe306, βSer308, and βGly232, emphasizing the importance of loop βL8 (βHis260−βVal309) in cation binding.

Woehl and Dunn (*45*) have raised the question whether the cation has a structural or a dynamic role. In the structural model, the metal changes the equilibrium constant for interconversion of active and inactive forms of the enzyme, whereas in the dynamic model the metal ion changes the relative position of transition-state vs ground-state energies and thereby produces a different set of the rate constants for the metal-free and metal-bound forms. In either model, the metal serves to allosterically fine-tune the catalytic machinery of the α- and β-active sites and the communication between them.

The TRPS complexes presented here show a new feature of the metal dependency of TRPS, namely, the enzymatically induced loss of the cation. In the $TRPS^{IPP}$ structure the sodium binding site is very well-defined and the observed quadratic pyramidal coordination (2.4−2.7 Å) by the βPhe306, βSer208 and βGly232 carbonyl oxygen atoms and two water molecules is the same as for the unligated TRPS (*24*). The $TRPS^{IPP}$ structure shows in great detail the allosteric pathway between the α- and β-active sites mediated by the COMM-domain via the—not only literally—central metal binding site.

Although the $TRPS^{IPP}$ and the $TRPS^{IGP}$ complexes were prepared identically, save the respective α-site ligand, the refined $TRPS^{IGP}$ complex lacks electron density for a metal ion (Figure 5). The reason for the modified cation binding site is the large IGP induced COMM domain movement leading to the open β-subunit in $TRPS^{IGP}$. This movement disrupts the hydrogen bond pattern that links several residues of the COMM domain to residues involved in ion binding or to residues interacting with these. This results in a narrowing of the metal binding loop and thus a loss of the sodium ion. These findings may explain why the α-activity is higher in the absence of monovalent cations (*45*). In addition, the observation of two conformations of parts (βGlu295−βSer297, βAsp305−βPro307) of the metal binding loop βL8 in the $TRPS^{IPP}$ structure (with the majority conformation having the metal bound, the minority conformation being the same as in the IGP complex) indicates an equilibrium distribution between two states of the enzyme.

This might be related to the results of Woehl and Dunn (*20*, *21*) who find two slowly converting forms of TRPS.

Changes near the β-Active Site upon IGP Binding. A further conformational change upon IGP binding to the α-site occurs at the highly conserved glutamine βGln114 that is located in the COMM domain (Figure 5). In TRPS^{IPP}, the βGln114 amino nitrogen $N_{\epsilon 2}$ hydrogen bonds directly to the βGly83 carbonyl oxygen atom (3.0 Å), and via a water molecule (2.8 Å) to the βThr88-$O_{\gamma 1}$ oxygen (2.8 Å) and the βAla85 carbonyl oxygen (3.0 Å). The carbonyl oxygen atom $O_{\epsilon 1}$ of βGln114 interacts with βAsn145-$N_{\delta 2}$ via another water molecule. This side chain conformation of βGln114 is conserved in all TRPS complexes described so far (including TRPS-αD60N^{IGP}), irrespective of the chemical nature of the bound ligand(s) or of a mutation. Although some of these complexes lack some of the water-mediated hydrogen bonds, which we attribute to the lower resolution of the respective structure, the direct hydrogen bond to the βGly83 carbonyl oxygen is conserved throughout.

Because of the displacement of the COMM domain in the TRPS^{IGP} complex, the βGln114-C_α atom moves by 1.1 Å. The backbone movements of the N-terminal site of helix βH4 (residues βGly113−βAla118), of the preceding sheet βS3 (βIle107−βThr110), and of loop βL3 (βGly111−βAla112) prevent the formation of the hydrogen bonds described above, leading to a rotation of βGln114. Interestingly, in the new conformation, the βGln114 side chain amide group is positioned roughly above (∼4.0 Å) and parallel to N_ξ of the Schiff base linkage of the internal aldimine formed by βLys87 and PLP (Figure 5). This conformation may allow interaction of the lone pair electrons of the $O_{\epsilon 1}$ carbonyl oxygen atom of βGln114 and the empty p-orbital of the positively charged nitrogen atom of the Schiff base. The amino nitrogen $N_{\epsilon 2}$ of βGln114 forms a hydrogen bond to a water molecule (2.7 Å), which in turn interacts with O_{3A} of PLP. This latter interaction may stabilize the negative charge at this oxygen atom. The conformational change of βGln114 may render the internal aldimine of the pyridoxal phosphate more susceptible for the nucleophilic attack by serine.

Implications for the Mechanism. A key feature of the allosteric interaction between the active sites of the α- and β-subunits is believed to be their switching between "open" and "closed" states (*1*, *5*, *12*, *26*). These are characterized by their propensity to bind substrates (with the open state having high affinity) and to catalyze the respective reactions (with the closed state being catalytically competent). Accordingly, unligated TRPS is believed to have both active sites in the open conformation, whereas the aminoacrylate complex of the IGP complexed TRPS represents the state with both subunits in the closed conformation. Partially closed states correspond to low activity states, such as the external aldimine complexes of the β subunit (*12*). A similar feature is observed at the α-active site where an isomerization of the IGP complex (TRPS^{IGP}) to a catalytically active form (TRPS^{IGP*}) takes place (*5*). Our TRPS^{IGP} structure corresponds to the pre-isomerized, partially closed α-state that represents a low-activity form of the α-active site. Interestingly, it is only this form that induces at the β-active site an open state (and not partially open as observed in the IPP or GP complexes) in which the cofactor PLP is accessible from the solvent (Figure 7). Since serine binds to PLP, the structure suggests a structural explanation of the observation that IGP binding to the α-site increases the affinity of serine to the β-active site (*12*). Its reactivity toward serine may be modulated by the new conformation of βGln114 induced by the large IGP induced COMM domain movement in the wild-type enzyme as described above. In this new conformation, the side chain of βGln114 would be close (3.3 Å) to the serine nitrogen atom of the external aldimine (as inferred from the wild-type TRPS^{F-IPP} aminoacrylate complex (*14*)) and could stabilize charges at the intermediate.

In addition to a closed COMM-domain conformation (*14*), we postulate a further conformational change at the IGP complexed α-site upon formation of the aminoacrylate intermediate, known to be the chemical signal that triggers the conformational transition that activates the α-reaction (*5*, *12*, *46*). This second conformational change, corresponding to the kinetically observed isomerization of the TRPS^{IGP} complex (*5*), is a direct consequence of the structural data presented here. In the TRPS^{IGP} complex, αGlu49 forms a hydrogen bond that is suitable for proton abstraction from the C3′-hydroxyl group of the IGP ligand, but αAsp60 forms only a weak hydrogen bond to the indole nitrogen atom. Thus, we predict a second side-chain movement of αAsp60 combined with a reorientation of the IGP molecule to allow for loop αL6 closure while avoiding the steric clash between the C2′-hydroxyl group and the αThr183-$C_{\gamma 2}$ side-chain carbon atom. Although structures of mutant complexes of TRPS have proven to be problematic in terms of mechanistic interpretation (see (*14*), for the discussion of the TRPS-βK87T structures, and this work for TRPS-αD60N) due to the intricate network of interactions between the active sites, the assumption of a second conformational change would be in agreement with the structure of the GP complex; in the TRPS-βK87T^{GP} structure (*15*), which displays a closed αL6 loop, the propane moiety adopts a different conformation than in the TRPS^{IGP} complex.

The structures of the TRPS^{IGP} and the TRPS^{IPP} complexes presented here also allow to address a problem discussed recently (*20*), namely, the finding of closed α- and β-active sites in the GP or IPP complexes of the external aldimine of TRPS-βK87T (*15*). Since the α-site should be in the low activity state in this complex, Woehl and Dunn suggest that these structures are more likely to represent the partially closed state. Our TRPS^{IGP} and TRPS^{IPP} structures show first, what the conformation of the partially closed form looks like, and second, that IPP complexes most likely represent "artificially" closed low activity states that are unlikely to be of direct catalytic relevance.

ACKNOWLEDGMENT

We thank Karen S. Anderson for the generous gift of IPP, Sonja Hönig for expert technical assistance, Axel Müller for help with the IGP synthesis, Thomas R. Schneider for stimulating discussions, Roger S. Goody and Robert M. Sweet for continuous encouragement and support. I.S. is extremely grateful for the generous support by the Richard und Anne-Liese Gielen-Leyendecker Stiftung.

REFERENCES

1. Pan, P., Woehl, E., and Dunn, M. F. (1997) *TIBS 22*, 22−27.
2. Miles, E. W. (1995) *Sub-Cellular Biochem. 24*, 207−254.
3. Miles, E. W. (1991) *Adv. Enzymol. Relat. Areas Mol. Biol. 64*, 93−172.

4. Ovadi, J. (1991) *J. Theor. Biol. 152*, 135−141.
5. Anderson, K. S., Miles, E. W., and Johnson, K. A. (1991) *J. Biol. Chem. 266*, 8020−8033.
6. Hyde, C. C., Ahmed, S. A., Padlan, E. A., Miles, E. W., and Davies, D. R. (1988) *J. Biol. Chem. 263*, 17857−17871.
7. Liang, P. H., and Anderson, K. S. (1998) *Biochemistry 37*, 12195−12205.
8. Welch, G. R., and Easterby, J. S. (1994) *TIBS 19*, 193−197.
9. Holden, H. M., Thoden, J. B., and Raushel, F. M. (1998) *Curr. Opin. Struct. Biol. 8*, 679−685.
10. AE, v. A., Seger, K., Turley, S., Sokatch, J. R., and Hol, W. G. (1999) *Nat. Struct. Biol. 6*, 785−792.
11. Miles, E. W., Rhee, S., and Davies, D. R. (1999) *J. Biol. Chem. 274*, 12193−12196.
12. Brzovic, P. S., Ngo, K., and Dunn, M. F. (1992) *Biochemistry 31*, 3831−3839.
13. Leja, C. A., Woehl, E. U., and Dunn, M. F. (1995) *Biochemistry 34*, 6552−6561.
14. Schneider, T. R., Gerhardt, E., Lee, M., Liang, P. H., Anderson, K. S., and Schlichting, I. (1998) *Biochemistry 37*, 5394−5406.
15. Rhee, S., Parris, K. D., Hyde, C. C., Ahmed, S. A., Miles, E. W., and Davies, D. R. (1997) *Biochemistry 36*, 7664−7680.
16. Nagata, S., Hyde, C. C., and Miles, E. W. (1989) *J. Biol. Chem. 264*, 6288−6296.
17. Rhee, S., Miles, E. W., Mozzarelli, A., and Davies, D. R. (1998) *Biochemistry 37*, 10653−10659.
18. Kayastha, A. M., and Miles, E. W. (1991) *Anal. Biochem. 193*, 200−203.
19. Rhee, S., Parris, K. D., Ahmed, S. A., Miles, E. W., and Davies, D. R. (1996) *Biochemistry 35*, 4211−4221.
20. Woehl, E., and Dunn, M. F. (1999) *Biochemistry 38*, 7118−7130.
21. Woehl, E., and Dunn, M. F. (1999) *Biochemistry 38*, 7131−7141.
22. Woehl, E. U., and Dunn, M. F. (1995) *Coord. Chem. Rev. 144*, 147−197.
23. Peracchi, A., Mozzarelli, A., and Rossi, G. L. (1995) *Biochemistry 34*, 9459−9465.
24. Hyde, C. C., Parris, K. D., Bhat, T. N., Brown, C., Ahmed, S. A., Miles, E. W., and Davies, D. R. (1999) to be published.
25. Yutani, K., Ogasahara, K., Tsujita, T., Kanemoto, K., Matsumoto, M., Tanaka, S., Miyashita, T., Matsushiro, A., Sugino, Y., and Miles, E. W. (1987) *J. Biol. Chem. 262*, 13429−13433.
26. Kirschner, K., Lane, A. N., and Strasser, A. W. (1991) *Biochemistry 30*, 472−478.
27. Rhee, S., Miles, E. W., and Davies, D. R. (1998) *J. Biol. Chem. 273*, 8553−8555.
28. Miles, E. W., Kawasaki, H., Ahmed, S. A., Morita, H., and Nagata, S. (1989) *J. Biol. Chem. 264*, 6280−6287.
29. Kawasaki, H., Bauerle, R., Zon, G., Ahmed, S. A., and Miles, E. W. (1987) *J. Biol. Chem. 262*, 10678−10683.
30. Kabsch, W. (1993) *J. Appl. Crystallogr. 26*, 795−800.
31. Brünger, A. T., Adams, P. D., Clore, G. M., DeLano, W. L., Gros, P., Grosse-Kunstleve, R. W., Jiang, J.-S., Kuszewski, J., Nilges, M., Pannu, N. S., Read, R. J., Rice, L. M., Simonson, T., and Warren, G. L. (1998) *Acta Cryst. D54*, 905−921.
32. Collaborative Computational Project, N. 4. (1994) *Acta Crystallogr. D50*, 760−763.
33. Murshudov, G. N., Vagin, A. A., Lebedev, A., Wilson, K. S., and Dodson, E. J. (1999) *Acta Crystallogr. D55*, 247−255.
34. Jones, T. A., Zou, J. Y., Cowan, S. W., and Kjelgaard, M. (1991) *Acta Crystallogr. A47*, 110−119.
35. Brünger, A. T., Krukowski, A., and Erickson, J. (1990) *Acta Crystallogr. A46*, 585−593.
36. Tronrud (1992) *Acta Crystallogr. A48*, 912−916.
37. Lamzin, V. S., and Wilson, K. S. (1993) *Acta Crystallogr. D49*, 129−147.
38. Schomburg, D., and Reichelt, J. (1988) *J. Mol. Graphics 6*, 161−165.
39. Ogasahara, K., Sawada, S., and Yutani, K. (1989) *Proteins 5*, 211−217.
40. Miles, E. W., Mcphie, P., and Yutani, K. (1988) *J. Biol. Chem. 263*, 8611−8614.
41. Ahmed, S. A., Hyde, C. C., Thomas, G., and Miles, E. W. (1987) *Biochemistry 26*, 5492−5498.
42. Mozzarelli, A., Peracchi, A., Rossi, G. L., Ahmed, S. A., and Miles, E. W. (1989) *J. Biol. Chem. 264*, 15774−15780.
43. Kabsch, W., and Sander, C. (1983) *Biopolymers 22*, 2577−2637.
44. Ruvinov, S. B., Ahmed, S. A., Mcphie, P., and Miles, E. W. (1995) *J. Biol. Chem. 270*, 17333−17338.
45. Woehl, E. U., and Dunn, M. F. (1995) *Biochemistry 34*, 9466−9476.
46. Banik, U., Zhu, D. M., Chock, P. B., and Miles, E. W. (1995) *Biochemistry 34*, 12704−12711.
47. Kraulis, P. J. (1991) *J. Appl. Crystallogr. 24*, 946−950.
48. Bacon, D. J., and Anderson, W. F. (1988) *J. Mol. Graphics 6*, 219−220.
49. Merritt, E. A., and Murphy, M. E. P. (1994) *Acta Crystallogr. D50*, 869−873.
50. Esnouf, R. M. (1997) *J. Mol. Graphics 15*, 132−134.
51. Nicholls, A., Sharp, K., and Honig, B. (1991) *Proteins 11*, 281−296.

BI9920533